International Journal of Quantum Chemistry

WILEY

International Journal of QUANTUM CHEMISTRY

RESEARCH ARTICLE

Adsorption Behavior of Phenyl-Substituted Cyclopropanecarboxylic Acid on Al and Cu Surfaces: A Combined Experimental and First-Principles Study

Tuncay Karakurt[1] | Alaaddin Cukurovali[2] | Ibrahim Yilmaz[3,4]

[1]Department of Chemical Engineering, Faculty of Engineering-Architecture, Kırsehir Ahi Evran University, Kirsehir, Turkey | [2]Department of Chemistry, Faculty of Science, Firat University, Elazig, Turkey | [3]Department of Mathematics and Science Education, Faculty of Education, Bolu Abant İzzet Baysal University, Bolu, Turkiye | [4]Innovative Food Technologies Development Application and Research Centre, Bolu Abant İzzet Baysal University, Bolu, Turkiye

Correspondence: Tuncay Karakurt (tuncaykarakurt@gmail.com)

Received: 26 March 2025 | **Revised:** 1 June 2025 | **Accepted:** 23 June 2025

Funding: The authors received no specific funding for this work.

Keywords: adsorption | CP2K | density functional theory (DFT) | Gaussian | IR | metal surfaces | NMR | organic molecules | phenyl-substituted Cyclopropanecarboxylic acid | X-ray crystallography

ABSTRACT

The molecular structure of phenyl-substituted cyclopropanecarboxylic acid (PSCCA, $C_{12}H_{14}O_2$; *3-methyl-3-phenylcyclobutane-1-carboxylic acid*) was determined using nuclear magnetic resonance (NMR), infrared spectroscopy (IR), and X-ray crystallography techniques. Following structural confirmation, its molecular geometry was optimized at the Density Functional Theory (DFT) level. The van der Waals interactions were accurately accounted for using the DFT-D3 method in the CP2K program. Understanding the adsorption behavior of organic molecules on metal surfaces is of great significance for applications in catalysis, sensor design, surface functionalization, and corrosion prevention. In this context, the adsorption properties of the PSCCA molecule on Al and Cu surfaces were investigated in detail using DFT-based CP2K calculations. By optimizing different adsorption configurations, the binding energies of the most stable structures were calculated and compared. The obtained results indicate that the PSCCA molecule strongly binds to both Al and Cu surfaces, with a higher adsorption energy on the Al surface compared to the Cu surface. In addition, Mulliken population analysis revealed distinct electronic charge transfer characteristics upon adsorption, with substantially stronger electron transfer observed on the Cu(111) surface due to enhanced d-band–ligand orbital hybridization. This electronic behavior correlates with the adsorption strength and highlights the critical role of metal electronic structure in governing surface interactions. Electron density difference analyses suggest that PSCCA interacts with both surfaces via a physisorption mechanism. Furthermore, assessments in the context of surface inhibitor efficiency reveal that PSCCA has the potential to passivate active surface regions and hinder surface reactions. Analyses conducted under different pH conditions indicate that the inhibitory effect of PSCCA is particularly pronounced in acidic environments. These findings suggest that PSCCA, exhibiting higher adsorption energy and stability on the Al surface, can be considered an effective protective agent and may play a crucial role in the design of metal–organic interfaces.

1 | Introduction

Cyclopropane derivatives have long attracted significant interest in organic and medicinal chemistry due to their unique structural features, ring strain, and reactivity profiles. Among them, cyclopropanecarboxylic acids represent an important class of compounds, often serving as versatile intermediates in the synthesis of pharmaceuticals, agrochemicals, and functional materials [1]. Incorporation of a phenyl group at the cyclopropane ring further enhances the chemical and biological properties of these molecules by introducing additional conjugation and steric effects, making phenyl-substituted cyclopropanecarboxylic acids (PSCCA) valuable scaffolds for the development of novel bioactive molecules [2]. The phenyl group not only stabilizes the cyclopropane moiety but also modulates the acidity of the carboxyl group and the molecule's overall lipophilicity, which plays a crucial role in drug design and receptor binding interactions [3]. Furthermore, the strained cyclopropane ring can undergo various ring-opening reactions under appropriate conditions, providing access to diverse functionalized compounds [4]. In recent years, significant progress has been made in the synthesis and functionalization of PSCCAs through methodologies such as metal-catalyzed cyclopropanation, carbene transfer reactions, and asymmetric catalysis [5]. These advances not only expand the synthetic utility of these compounds but also open new avenues for their application in medicinal chemistry and material science. PSCCAs have attracted considerable attention due to their diverse range of applications in medicinal chemistry, asymmetric synthesis, and materials science. In medicinal chemistry, the rigid and strained cyclopropane ring imparts metabolic stability and resistance to enzymatic degradation, making these compounds valuable in drug design [1, 3]. The presence of the phenyl group enhances lipophilicity and allows for favorable π–π stacking interactions with biological targets, thereby improving binding affinity and specificity. Several bioactive molecules incorporating PSCCA frameworks have demonstrated promising pharmacological activities. For instance, derivatives of 2-phenylcyclopropanecarboxylic acid have shown inhibitory effects on cyclooxygenase (COX) enzymes, indicating potential anti-inflammatory properties [3]. Moreover, specific analogues have been evaluated as GABA receptor modulators and antiviral agents, further highlighting their versatility in therapeutic applications [2, 4]. In addition to their medicinal relevance, PSCCAs serve as important chiral building blocks in organic synthesis. Their defined stereochemistry allows for the preparation of enantiomerically pure intermediates, which are crucial in the synthesis of natural products, peptide mimetics, and chiral ligands [2, 5]. The functionalizable carboxyl group and phenyl ring further enable structural diversification, providing access to a wide array of complex molecules. Beyond the field of pharmaceuticals, these compounds also find utility in the development of advanced materials and agrochemicals. Their rigid three-membered ring structure contributes to the synthesis of polymers with enhanced mechanical strength and thermal stability [1]. Furthermore, certain derivatives exhibit biological activity as herbicides and pesticides, offering practical applications in the agricultural sector [4]. The structural elucidation of PSCCAs is typically achieved through a combination of spectroscopic and crystallographic techniques. Nuclear magnetic resonance (NMR) spectroscopy provides detailed information about the molecular framework and stereochemistry, while Infrared (IR) spectroscopy aids in the identification of functional groups, particularly the carboxyl moiety. Additionally, X-ray diffraction (XRD) analysis plays a crucial role in determining the precise crystal structure, confirming the arrangement of atoms within the molecule. Beyond experimental characterization, understanding the interaction of these molecules with metal surfaces is of significant interest, especially in catalysis and materials science. Investigating the adsorption behavior of PSCCAs on metallic substrates provides insights into their surface chemistry and potential applications. In this study, we explore the adsorption properties of PSCCA on aluminum (Al) and copper (Cu) surfaces.

2 | Material and Methods

2.1 | X-Ray Measurements and Refinement

Single-crystal XRD data were collected using a Bruker AXS APEX CCD diffractometer with MoKα radiation [6]. The initial crystal structure was determined via direct methods utilizing the SHELXT program [7]. Refinement of the positions of non-hydrogen atoms was performed using the full-matrix least squares method within the SHELXL software [8]. Both isotropic and anisotropic refinements were applied to accurately model these atomic positions. Hydrogen atoms bonded to carbon atoms were placed in calculated positions based on standard geometries, with C–H bond lengths set to 0.93 Å for aromatic, 0.97 Å for methylene, and 0.96 Å for methyl groups. The hydrogen atom attached to the nitrogen atom was located from a difference Fourier map and refined isotropically, with the O–H bond distance restrained to 0.84 Å. It has been determined that one of the oxygen atoms (O_2) is located in two distinct positions within the structure. From a crystallographic symmetry perspective, this oxygen atom was modeled in two different positions, and the site occupancy factors of these positions were freely refined. The refined occupancy factors were found to be 0.483 (5) for atom O2A and 0.517 (5) for atom O2B, indicating that the oxygen atom is distributed approximately equally between the two positions, thereby confirming the presence of positional disorder in the structure. An examination of the refined geometric parameters reveals that the bond lengths and bond angles associated with the disordered fragments remain within chemically acceptable limits. Additionally, the thermal parameters of the relevant atoms exhibit physically meaningful values, ensuring that no overparameterization issues arise in the structural model. Analysis of the final difference Fourier map indicates that no significant residual electron density is observed around the disordered oxygen atoms. The highest residual electron density peak in the refined structure is +0.30 e Å^{-3}, located approximately 0.97 Å from the regularly positioned O1 atom in the crystal. This value falls within the acceptable range for crystal structure determination and does not suggest the necessity of an additional disorder model or the presence of an unresolved solvent molecule. Further structure refinement and analysis were carried out using the Olex2 software package [9], while molecular illustrations were prepared using Mercury.

2.2 | Synthesis and Crystallization

In a three-necked flask equipped with a thermometer, a dropping funnel, and a magnetic stirrer was charged with 16 g NaOH and

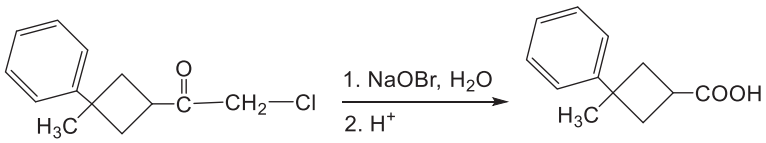

SCHEME I | Reaction sequence for synthesis of the title compound.

8 mL water. The system was cooled to 0°C. A quantity of 20 g of Br_2 solution dissolved in 40 mL of dioxane is added dropwise so that the temperature does not exceed 10°C. Then the flask is cooled back to 0°C, and 9 g of α-haloketone [10] dissolved in dioxane is added in such a way that the temperature does not exceed 10°C. The reaction mixture was stirred at 30°C–35°C for 3 h. The mixture obtained is extracted three times with 150–200 mL of ether. Ether was evaporated in a rotary evaporator. The obtained precipitate was triturated with water and acidified with 5% H_2SO_4, filtered off, washed with plenty of water, and crystallized from ethanol (Scheme I). Yield: 28%. M.p.: 390 K. IR (KBr, υ cm^{-1}): 3083 and 3031 (aromatics), 2962–2863 (aliphatics), 1698 (C=O). ^{1}H NMR ($CDCl_3$, TMS, δ ppm): 1.53 (s, 3H, $-CH_3$ on cyclobutane ring), 2.38–2.43 (m, 2H, $-CH_2-$, in cyclobutane ring), 2.66–2.71 (m, 2H, $-CH_2-$, in cyclobutane ring), 3.35 (quint, $j = 9.2$ Hz, 1H, > CH– in cyclobutane ring), 7.17–7.21 (m, 3H, aromatics), 7.33–7.36 (m, 2H, aromatics), 10.07 (brs, 1H, –OH). ^{13}C NMR ($CDCl_3$, TMS, δ ppm): 181.53, 151.04, 128.32, 125.64, 124.55, 38.81, 37.19, 32.29, and 29.95.

2.3 | Computational Details

The adsorption of PSCCA on aluminum (Al) and copper (Cu) surfaces was investigated using density functional theory (DFT)-based calculations performed with the CP2K software package [11]. All calculations included dispersion corrections using Grimme's DFT-D3 [12] method, which enables a more accurate treatment of van der Waals interactions often underestimated in conventional DFT.

The metal surfaces were modeled as periodic slabs representing the (111) facets of both Al and Cu, as these are the most thermodynamically stable and widely exposed low-index surfaces of FCC metals, providing a realistic representation for adsorption studies. Aluminum and copper were selected due to their industrial relevance in corrosion inhibition, catalysis, and surface functionalization applications. Each surface was constructed using a four-layer slab model, with the bottom two layers fixed and the top two layers relaxed. A vacuum spacing of 15 Å was included along the z-axis to prevent interactions between periodic images.

The PSCCA molecule was initially placed in multiple orientations above each surface to identify the most favorable adsorption configuration. Geometry optimizations were carried out using the Gaussian and Plane Waves (GPW) method. The Perdew-Burke-Ernzerhof (PBE) exchange-correlation functional [13] with GTH-PBE pseudopotentials and the DZVP-MOLOPT-SR-GTH basis set [14] was employed for all atoms. A plane-wave cutoff energy of 400 Ry was used.

The adsorption energy (E_{ads}) was calculated according to the following equation:

$$E_{ads} = E_{total} - (E_{surface} + E_{molecule})$$

where E_{total} represents the total energy of the molecule-surface system, $E_{surface}$ is the energy of the clean metal surface, and $E_{molecule}$ denotes the energy of the isolated molecule.

Solvent effects were modeled explicitly for both water and hydrochloric acid. In the water-solvated systems, 150 H_2O molecules were introduced around the adsorbed PSCCA molecule. In the hydrochloric acid-solvated systems, 130 HCl molecules were used. These explicit solvent molecules were placed to simulate localized solvation environments. All calculations were performed as static geometry optimizations, and no molecular dynamics (MD) simulations were conducted.

All structures and outputs were visualized using VMD and CP2K tools, and selected data were processed with in-house Python scripts.

3 | Results and Discussion

3.1 | Geometrical Structure of Title Compound

The molecular formula of the compound is $C_{12}H_{14}O_2$, with a molecular weight of 190.23 g/mol. The crystal system of the structure is monoclinic, and it is classified within the space group $P2_1/n$. The unit cell parameters were determined as follows: $a = 6.0510$ (13) Å, $b = 7.4428$ (18) Å, $c = 23.682$ (6) Å, $\alpha = 90°$, $\beta = 97.078$ (9)°, and $\gamma = 90°$. These parameters confirm the distinctly monoclinic nature of the crystal. The unit cell volume was calculated as 1058.4 (4) Å^3, with four molecules per unit cell ($Z = 4$). The calculated density of the structure is 1.194 g/cm^3, and measurements were conducted using MoKα radiation ($\lambda = 0.71073$ Å). A total of 15 557 reflections were collected, of which 2588 were identified as independent reflections. The R_int and R_sigma values were determined as 0.0398 and 0.0394, respectively. Structural solution and refinement were performed using the Olex2 interface with the SHELXD and SHELXL programs. The refinement process yielded a well-fitted structure, with the highest peak and deepest hole in the residual electron density map at 0.30 and −0.24 eÅ^{-3}, respectively. The difference Fourier electron density map (Figure 1) revealed no significant residual density, further confirming the correctness of the obtained model and absence of unresolved features.

The final R indices were found to be $R_1 = 0.0643$ and $wR_2 = 0.1472$ for reflections with $I \geq 2\sigma(I)$, and $R_1 = 0.1136$ and $wR_2 = 0.1749$ for all data, indicating that the crystal structure is of sufficient quality. The crystal dimensions were measured as $0.11 \times 0.10 \times 0.08$ mm^3, with an absorption coefficient of 0.080 mm^{-1}. Suitable crystal dimensions were selected to

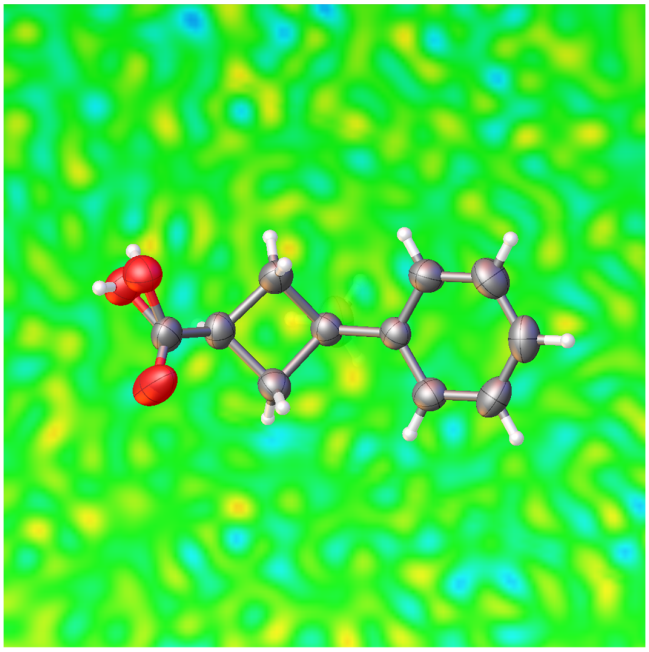

FIGURE 1 | Difference Fourier electron density map of the refined structure, showing no significant residual density.

ensure the acquisition of a high-quality dataset. During the refinement process, a total of 2588 data points, 18 restraints, and 141 parameters were utilized, resulting in a final goodness-of-fit (GooF) value of 1.049. These values confirm that the model is consistent with experimental data and provides reliable structural parameters. The results obtained from the crystal structure analysis accurately depict the three-dimensional arrangement of the molecule, supporting a crystal organization stabilized by hydrogen bonding and π−π stacking interactions. The determined structural parameters establish a robust foundation for further advanced analyses. In the crystal parameters of $C_{12}H_{14}O_2$ crystals, data collection and the details of the refinement process are given in Table 1.

A diagram of the molecule drawn, with experimental 20% probability ellipsoids, is given in Figure 2.

Crystal structure analysis has revealed that both hydrogen bonding and π−π stacking interactions significantly contribute to the overall stability of the structure. Within the molecular arrangement, the O2A hydroxyl group acts as a hydrogen bond donor, while the O1 carbonyl oxygen serves as an acceptor. The analysis indicates that the O−H···O hydrogen bond features an O···O distance of 2.679 Å, an H···O distance of 1.86 Å, and a bond angle of 173° (Table 2). These values suggest a nearly linear and strong hydrogen bonding characteristic, which facilitates the tight association of molecules. Additionally, PLATON analysis has identified a recurring bidirectional O1···O2A contact at a distance of 2.679 Å, supporting the formation of a chain-like network structure. Furthermore, pronounced π-π stacking interactions involving aromatic ring systems have been observed. The centroid-to-centroid distances between the Cg2 (C7−C12) ring centers were reported as 4.7678 (18) Å and 4.8274 (19) Å. The inter-ring angle was found to be 49.35°, while the Beta and Gamma values were approximately 14°−15°

TABLE 1 | Data collection and refinement values of the title crystal.

Empirical formula	$C_{12}H_{14}O_2$
Formula weight	190.23
Temperature/K	273.15
Crystal system	Monoclinic
Space group	$P2_1/n$
a/Å	6.0510 (13)
b/Å	7.4428 (18)
c/Å	23.682 (6)
α/°	90
β/°	97.078 (9)
γ/°	90
Volume/Å^3	1058.4 (4)
Z	4
ρ_{calc}g/cm^3	1.194
μ/mm^{-1}	0.080
F(000)	408.0
Crystal size/mm^3	0.11 × 0.1 × 0.08
Radiation	MoKα (λ = 0.71073)
2Θ range for data collection/°	3.466 to 56.504
Index ranges	$-8 \le h \le 7, -9 \le k \le 9, -31 \le l \le 31$
Reflections collected	15 557
Independent reflections	2588 [$R_{int} = 0.0398$, $R_{sigma} = 0.0394$]
Data/restraints/parameters	2588/18/140
Goodness-of-fit on F^2	1.049
Final R indexes [$I >= 2\sigma(I)$]	$R_1 = 0.0644$, $wR_2 = 0.1475$
Final R indexes [all data]	$R_1 = 0.1138$, $wR_2 = 0.1754$
Largest diff. peak/hole/e Å^{-3}	0.30/−0.24
CCDC	2 433 579

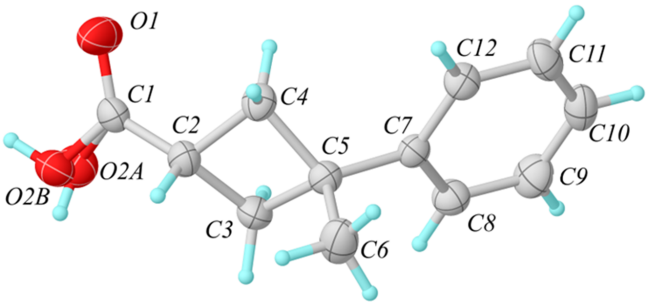

FIGURE 2 | Experimental figure of $C_{12}H_{14}O_2$ crystal.

and 63°−64°, respectively. These angular values indicate that the stacking interactions are not perfectly parallel but exhibit an offset arrangement. Additionally, the perpendicular distances between the rings were measured as 2.14 and 4.62 Å, highlighting a significant slippage distance between the aromatic systems. The intramolecular hydrogen bonding of the crystal is shown in Figure 3 and the representation of all interactions is shown in Figure 4.

TABLE 2 | Hydrogen Bonding and π-π Stacking Interactions in the Crystal Structure (Å, °).

Interaction type	Donor–acceptor/rings	Distances (Å)/centroid–centroid	Angles (°)	Contribution to structure
Hydrogen bonding	O2A–H2A ··· O1	O···O:2.679 H···O: 1.86	O–H···O angle: 173	Strong, directional hydrogen bonding; stabilization of the three-dimensional network
π–π stacking	Cg2 (C7–C12)···Cg2	Cg···Cg:4.768/4.827 CgI⊥:2.14 CgJ⊥: 4.62	α:49.35 β:14–15 γ: 63–64	Offset stacking arrangement; formation of a compact intermolecular structure

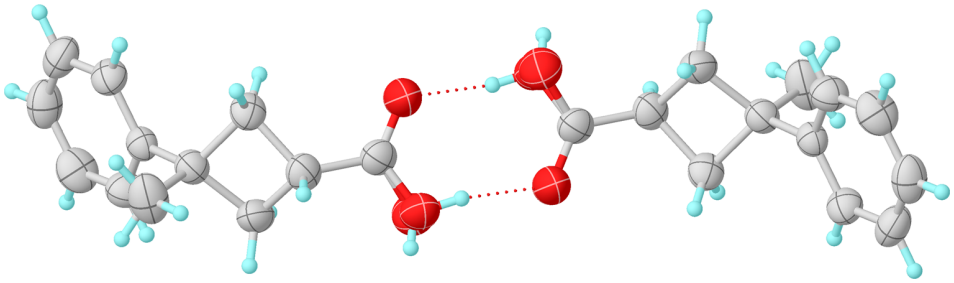

FIGURE 3 | A representation of the intermolecular O–H···O hydrogen bond.

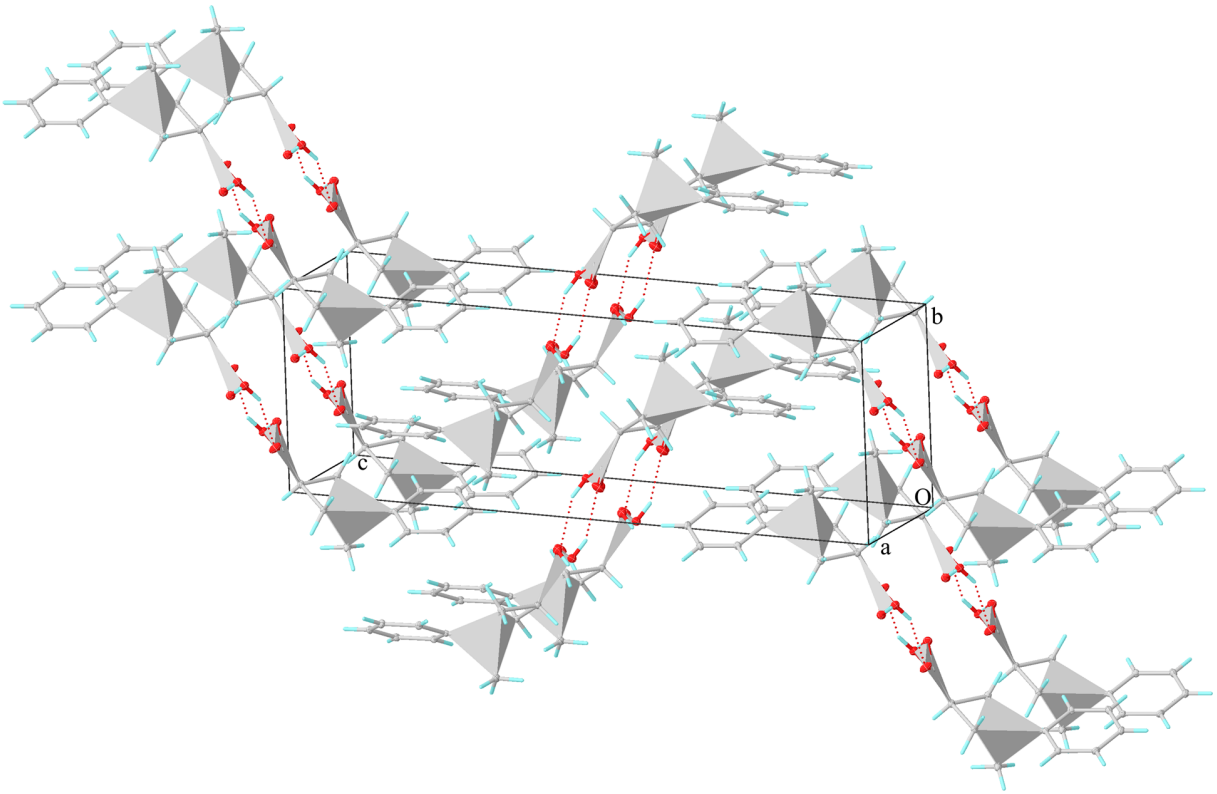

FIGURE 4 | Packaging of the crystal with O–H···O and π–π interactions along the *a*-axis.

Hydrogen bonds form a regular three-dimensional network between molecules through directional and strong interactions, while π–π stacking interactions enhance the compactness and stability of the structure due to the offset arrangement of aromatic rings. The chain-like structures formed by hydrogen bonds are supported by π–π stacking interactions, providing both linear and surface connections within the crystal lattice. These two types of interactions contribute synergistically to the overall stabilization of the crystal. In the crystal structure analysis conducted, the bond lengths (Table 3) and bond angles (Table 4) of the compound were carefully examined.

TABLE 3 | Bond lengths between atoms in the crystal structure.

		Length/Å				Length/Å	
Atom	**Atom**	**X-ray diffraction**	**DFT PBC**	**Atom**	**Atom**	**X-ray diffraction**	**DFT PBC**
O1	C1	1.207 (3)	1.24571	C1	C2	1.491 (3)	1.497
O2A	C1	1.280 (1)	1.32840	C1	O2B	1.346 (6)	—
C12	C7	1.389 (3)	1.39726	C5	C3	1.552 (3)	1.571
C12	C11	1.386 (3)	1.39682	C5	C6	1.533 (3)	1.536
C4	C5	1.558 (3)	1.57143	C2	C3	1.547 (3)	1.556
C4	C2	1.535 (3)	1.54817	C8	C9	1.376 (3)	1.398
C7	C5	1.511 (3)	1.51499	C11	C10	1.376 (4)	1.397
C7	C8	1.383 (3)	1.39726	C9	C10	1.376 (4)	1.397

TABLE 4 | Bond Angles between Atoms in the Crystal Structure.

			Angle/°					Angle/°	
Atom	**Atom**	**Atom**	**X-ray diffraction**	**DFT PBC**	**Atom**	**Atom**	**Atom**	**X-ray diffraction**	**DFT PBC**
C11	C12	C7	120.7 (2)	120.31	C7	C5	C6	109.70 (18)	110.31
C2	C4	C5	88.66 (16)	88.79	C3	C5	C4	87.66 (16)	88.72
C12	C7	C5	121.15 (19)	119.99	C6	C5	C4	111.27 (19)	110.61
C8	C7	C12	117.8 (2)	118.54	C6	C5	C3	111.88 (19)	111.56
C8	C7	C5	120.99 (19)	121.38	C4	C2	C3	88.66 (16)	89.58
O1	C1	O2A	120.6 (3)	121.53	C1	C2	C4	119.05 (18)	120.94
O1	C1	C2	123.4 (2)	123.60	C1	C2	C3	117.5 (2)	116.06
O1	C1	O2B	121.0 (3)	—	C2	C3	C5	88.46 (16)	87.98
O2A	C1	C2	114.0 (3)	112.65	C9	C8	C7	121.5 (2)	121.28
O2B	C1	C2	114.3 (3)	—	C10	C11	C12	120.4 (2)	120.55
C7	C5	C4	117.67 (17)	116.30	C10	C9	C8	120.2 (2)	119.75
C7	C5	C3	117.16 (18)	117.72	C11	C10	C9	119.4 (2)	119.52

The O1–C1 bond length was measured to be 1.206 (3) Å. This value is very close to the standard value of approximately 1.20 Å reported in the literature for the C=O double bond in a carbonyl group [15]. This confirms the classical strong π–bond character of the carbonyl function. The O2A–C1 bond was found to be 1.280 (5) Å, which, although shorter than the typical C–O single15bond length of approximately 1.36 Å, indicates the presence of resonance effects [16]. Similarly, the C1–O2B bond was measured to be 1.346 (6) Å, pointing to partial double bond character. The C–C bond lengths in the aromatic ring system range from 1.376 (3) Å to 1.390 (3) Å. These values are consistent with the expected 1.38–1.40 Å range for aromatic systems, supporting the delocalization of π–electrons [17, 18]. The C–C bond lengths observed in the aliphatic regions range from 1.491 (3) to 1.558 (3) Å, which are in close agreement with the expected 1.53–1.55 Å range for sp^3 hybridized carbons [19]. Regarding the bond angles, the O1–C1–O2A angle was found to be 120.6 (3)°, indicating the planarity of the sp^3 hybridized carbon atom. This value is consistent with the typical 120° values observed for carbonyl carbons [20]. The O1–C1–C2 and O1–C1–O2B angles were measured to be 123.4 (2)° and 121.0 (3)°, respectively, confirming the trigonal planar geometry. The bond angles observed in the aromatic ring ranged from 117° to 121°, aligning with values reported in the literature for aromatic systems [21]. The C–C–C bond angles in the aliphatic chain varied from 109° to 112°, reflecting tetrahedral geometry. Overall, the bond lengths and angles obtained from the crystal structure show a high degree of agreement with the average values reported in the literature. This suggests that the crystal lattice of the structure possesses stable geometry free from conformational strain.

3.2 | Periodic Boundary Calculations (PBC)

All geometry optimizations were performed under periodic boundary conditions (PBC) using the CP2K program package. The initial crystal structure was constructed based on experimental XRD data and placed in a triclinic simulation cell. The starting unit cell parameters were $a = 6.0510$ Å, $b = 7.4428$ Å, $c = 23.6820$ Å, $\alpha = 90°$, $\beta = 97.078°$, and $\gamma = 90°$, which accurately represent the experimental crystal environment. The periodic simulation cell contains 112 atoms per unit cell, fully

TABLE 5 | Comparison of the X-ray and optimized unit-cell parameters calculated by the cp2k-cell-opt method of the title crystal.

X-ray diffraction	DFT PBC
$a = 6.0510\ (13)$ Å	$a = 4.8078$ Å
$b = 7.4428\ (18)$ Å	$b = 8.2032$ Å
$c = 23.682\ (6)$ Å	$c = 22.5271$ Å
$\beta = 97.078\ (9)^{o}$	$\beta = 92.095^{o}$
$Z = 4$	$Z = 4$

representing the asymmetric molecular packing observed experimentally. The cell optimization was carried out using the Quickstep module within CP2K, employing a mixed Gaussian and plane-wave (GPW) approach. The exchange-correlation energy was described by the PBE functional, combined with DFT-D3 dispersion corrections to properly account for long-range van der Waals interactions. A plane-wave cutoff of 300 Ry and a tight electronic convergence threshold (EPS_DEFAULT = 1.0E−13) were applied to ensure accurate energy and force evaluations. During the optimization, both atomic positions and lattice parameters were allowed to relax under an applied external pressure of 1 atm using the DIRECT_CELL_OPT algorithm. Symmetry constraints were maintained (KEEP_SYMMETRY.TRUE.) to preserve the crystallographic space group. As a result of the periodic cell optimization, the unit cell parameters were refined to $a = 4.808$ Å, $b = 8.203$ Å, $c = 22.527$ Å, $\alpha = 90.050^{\circ}$, $\beta = 92.096^{\circ}$, and $\gamma = 89.974^{\circ}$. A detailed comparison between the optimized and experimental unit cell parameters is presented in Tables 3 and 4. The optimized cell dimensions exhibited reasonable agreement with the experimental values, reflecting minor anisotropic contractions and slight angular deviations, which are commonly attributed to functional-dependent systematic errors in DFT calculations.

In addition to the unit cell parameters, the optimized molecular geometry within the periodic environment was analyzed in detail. Bond lengths and bond angles obtained from the optimized structure were directly compared with experimental XRD data, and the comparative results are summarized in Table 5. The calculated geometrical parameters showed good agreement with the experimental measurements, confirming that the computational protocol accurately describes both intra- and intermolecular interactions under periodic boundary conditions. Furthermore, the experimental crystal structure (Figure 5a) and the DFT-optimized structure (Figure 5b) are presented for visual comparison. Both structures exhibit similar molecular conformations and packing motifs, further validating the reliability of the applied computational approach.

3.3 | Adsorption Energies of the Compound on Al (111) and Cu (111) Surfaces Under Different Conditions

The adsorption energies (ΔE) of five different conformations of the PSCCA molecule on the Al surface have been evaluated (Table 6).

The initial and optimized energy values presented in Figure 6 were analyzed to evaluate the structural stability of the Al–ligand complexes. The optimized energy values indicate that the system reaches a lower energy level, forming a more stable structure. In general, the optimized energy is lower than the initial energy, signifying that the complex becomes more stable. Among these conformations, the second conformation exhibits the most negative adsorption energy, with a value of −39.12 kcal/mol. This value represents the conformation in which the interaction between the molecule and the surface is the strongest, making the system the most stable. The first conformation, with an adsorption energy of −33.14 kcal/mol, demonstrates a stability close to that of the second conformation. In contrast, the adsorption energies of the third, fourth, and fifth conformations were calculated as −20.99, −25.42, and −17.90 kcal/mol, respectively, indicating weaker interactions.

Literature studies on the adsorption energies of organic molecules on aluminum surfaces have generally reported values within similar energy ranges. For instance, the adsorption energies of various organic molecules on Pd surfaces have been reported to range between −20 and −45 kcal/mol [22]. These findings reveal that variations in the binding mode of the molecule, particularly the positions of the carboxyl and phenyl groups, significantly influence the adsorption strength. Lower adsorption energies indicate that the molecule is positioned closer to the surface and forms stronger bonds [23]. This binding may primarily occur through electrostatic and potential covalent interactions. Overall, molecular conformation appears to be a key factor in determining surface adsorption behavior and system stability.

The adsorption behavior of the PSCCA molecule on the Cu surface was evaluated based on five different conformations (Table 7).

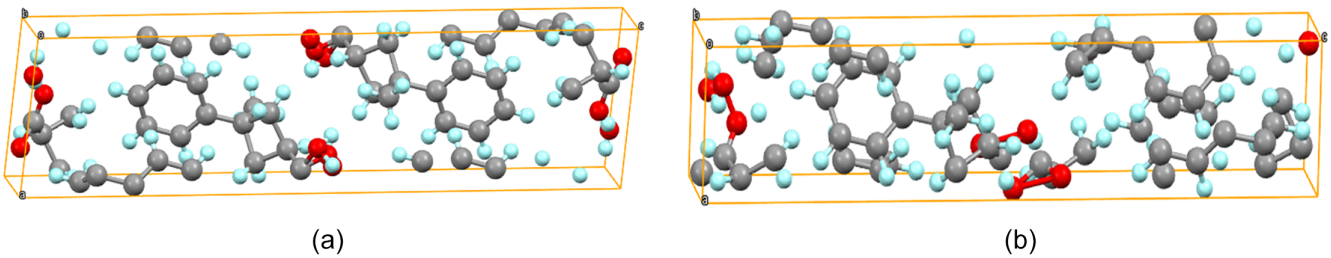

FIGURE 5 | Representation of atoms within the unit cell of the title crystal (a) X-Ray (b) DFT PBC.

TABLE 6 | Adsorption and total energies of Al–ligand complexes.

Conformation	E_{Al+lig}	E_{Al}	E_{lig}	ΔE (kcal/mol)
c1	−505.3376142	−396.6554907	−108.6293176	−33.1362
c2	−505.3471186	−396.6555127	−108.6292601	−39.1227
c3	−505.3192263	−396.6555235	−108.6302597	−20.9859
c4	−505.3251291	−396.655524	−108.629101	−25.4167
c5	−505.3144977	−396.6554627	−108.6305115	−17.8988

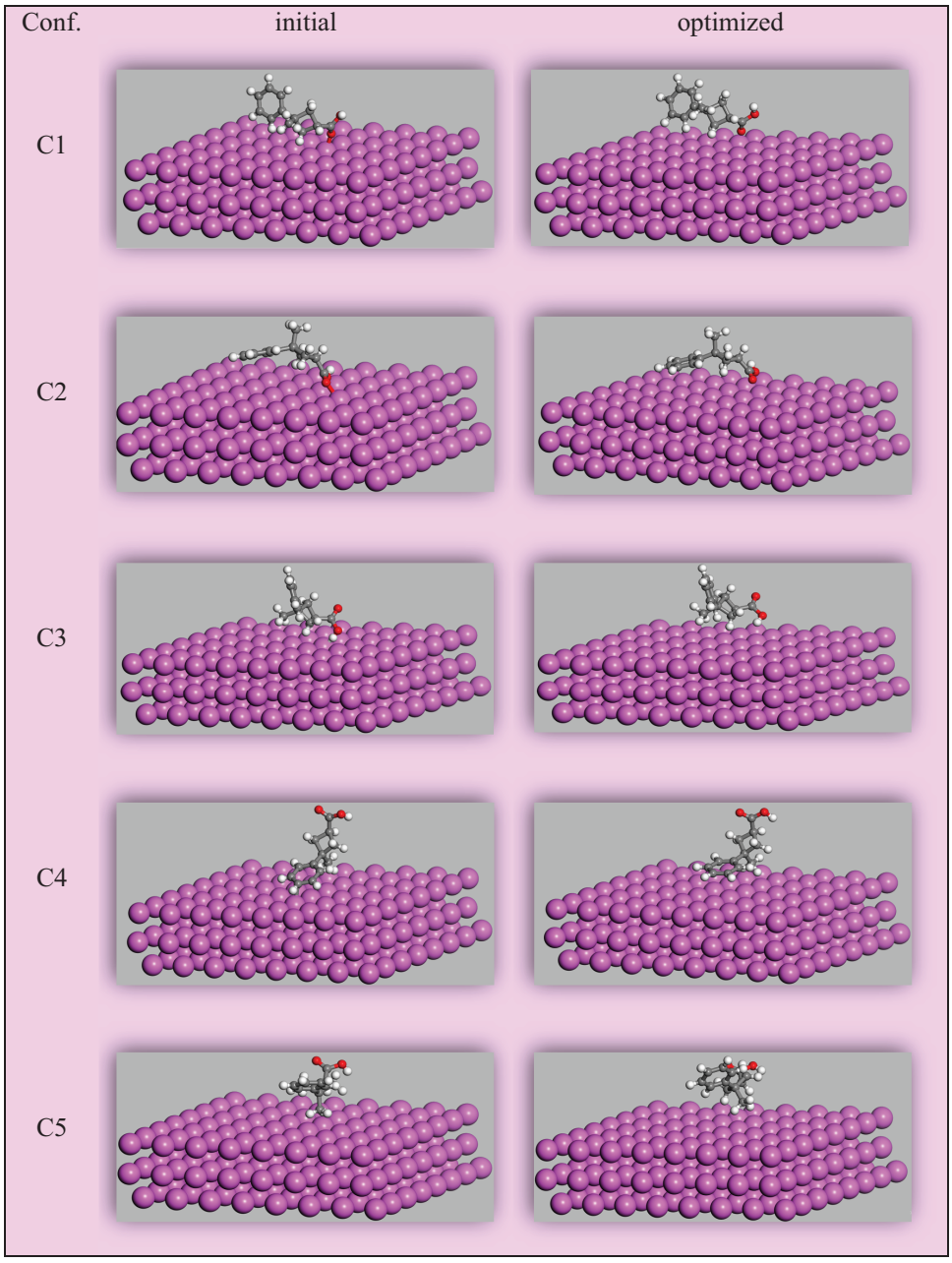

FIGURE 6 | Initial and optimized structures of Al–ligand conformers.

The initial and optimized conformations presented in Figure 7 were analyzed to evaluate the structural stability of the complexes. Calculations revealed that the lowest adsorption energy was obtained for the second conformation, with a value of −73.27 kcal/mol. This value indicates the conformation in which the interaction between the molecule and the surface is the strongest, making the system the most stable. The first conformation also exhibits high stability, with an adsorption energy

TABLE 7 | Adsorption and total energies of Cu–ligand complexes.

Conformation	E_{Cu+lig}	E_{Cu}	E_{lig}	ΔE (kcal/mol)
c1	−9348.522828	−9239.792093	−108.6235986	−67.229
c2	−9348.533590	−9239.792107	−108.6247162	−73.2728
c3	−9348.487801	−9239.792096	−108.6256202	−43.9789
c4	−9348.500792	−9239.792123	−108.6275589	−50.8975
c5	−9348.496628	−9239.792092	−108.628828	−47.5076

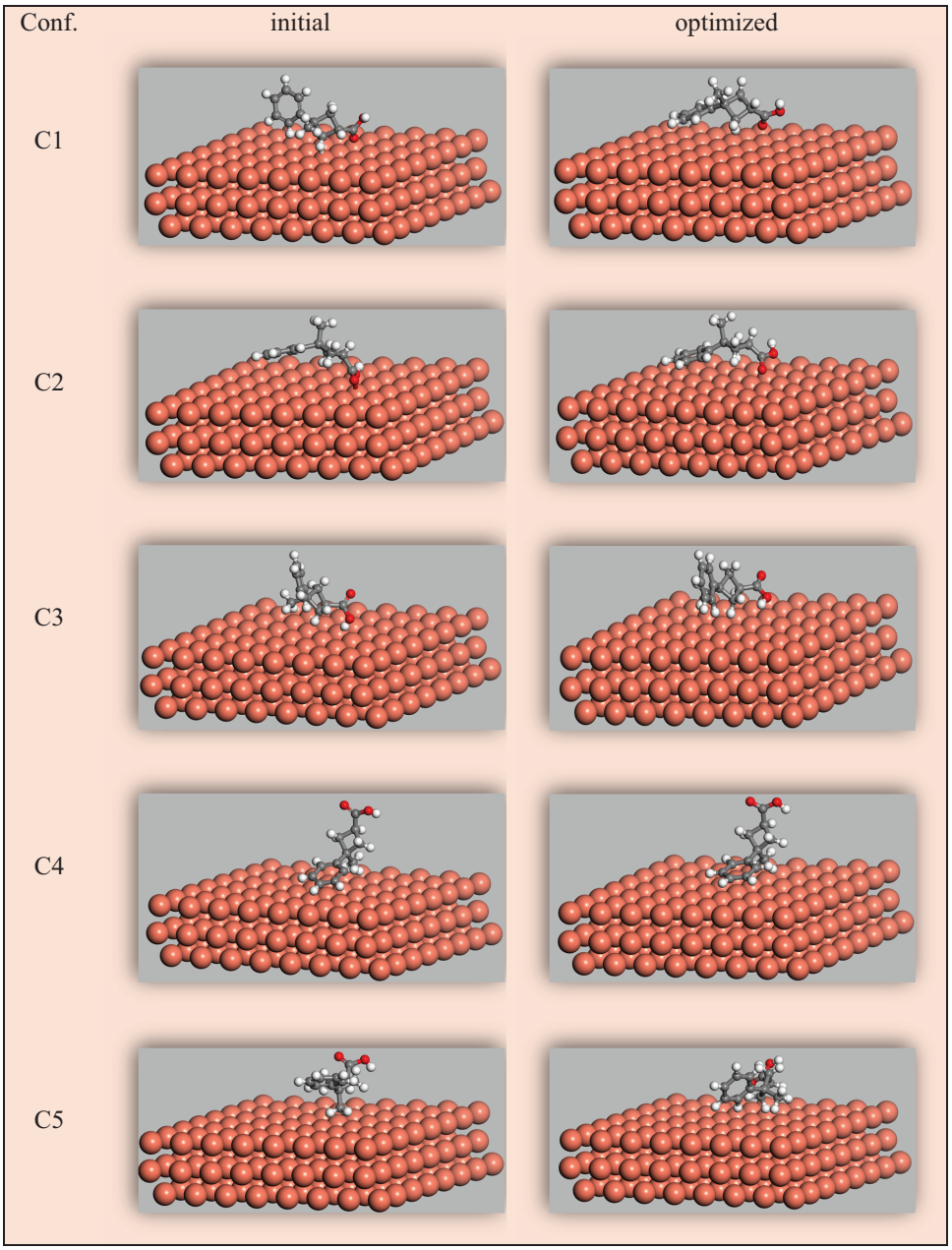

FIGURE 7 | Initial and optimized structures of Cu–ligand conformers.

of −67.23 kcal/mol. The third, fourth, and fifth conformations tend to bind more weakly, with adsorption energies of −43.98, −50.90, and −47.51 kcal/mol, respectively. The obtained results demonstrate that conformational changes play a crucial role in the interaction of the molecule with the surface. In particular, the proximity of the carboxyl group and the phenyl ring to the surface atoms emerges as a key factor in determining adsorption energy. More negative adsorption energy values indicate stronger binding of the molecule to the surface and greater thermodynamic stability of the system. Studies on the adsorption energies

TABLE 8 | Distances of O and C atoms and molecular *Z* values for Al–ligand complexes.

Conformation	Average O atom height (Å)	Minimum O atom height (Å)	Average C atom height (Å)	Minimum C atom height (Å)	Minimum molecular Z (Å)	Maximum molecular Z (Å)
C1	8.06	7.16	9.28	7.99	7.16	11.64
C2	7.40	7.30	8.70	7.87	7.30	11.37
C3	8.92	8.14	9.89	8.30	7.28	13.26
C4	13.13	13.00	9.16	7.79	7.34	13.25
C5	10.37	10.36	9.91	8.09	7.38	12.42

Note: Z axis: This is the axis perpendicular to the surface, indicating the vertical positioning of the molecule relative to the surface, that is, how far the molecule is located above or below the surface. Minimum Molecular *Z* (Å): This refers to the *z*-coordinate of the atom in the molecule that is closest to the surface (the atom at the lowest height). Maximum Molecular *Z* (Å): This refers to the *z*-coordinate of the atom in the molecule that is farthest from the surface (the atom at the highest position).

of organic molecules on copper surfaces have reported a wide range of values. For instance, the adsorption energy of benzene on the Cu (111) surface has been reported to be approximately −23.2 kcal/mol in the literature [24].

3.4 | Atomic Distance and Adsorption Behavior of the PSCCA Molecule on the Al(111) Surface

The adsorption behavior of five different conformations of the PSCCA molecule on the Al(111) surface was investigated, revealing significant differences in adsorption energies. Optimization calculations indicated that the lowest adsorption energy was obtained for the C2 conformation. In this configuration, the oxygen atoms of the carboxyl group were found to be positioned in close proximity to the surface. The average height of the oxygen atoms from the surface was determined to be 7.40 Å, with a minimum distance of 7.30 Å (Table 8). This finding suggests that electrostatic interactions between the molecule and the surface are particularly strong. Additionally, in the C2 conformation, the average height of the carbon atoms was approximately 8.70 Å, with the lowest carbon height recorded at 7.87 Å. The molecule was observed to adopt a slightly tilted position, aligning nearly parallel to the surface. This orientation indicates that both the oxygen atoms of the carboxyl group and the phenyl ring strongly interact with the surface. Consequently, the more negative adsorption energy of the C2 conformation compared to others suggests that the molecule is tightly bound to the surface, leading to greater thermodynamic stability. When evaluating the other conformations, it was observed that in the C1 conformation, the oxygen atoms were positioned slightly farther from the surface, with an average height of 8.06 Å and a minimum oxygen height of 7.16 Å. The average carbon atom height was 9.28 Å, indicating a more upright orientation relative to the surface. This configuration results in lower stability compared to C2. In the C3 conformation, the average height of the oxygen atoms was determined to be 8.92 Å, indicating a significantly greater distance from the surface. The average carbon height was calculated as 9.89 Å. The molecule's substantially distant and upright positioning weakened its interaction with the surface, thereby reducing system stability. Notably, in the C4 conformation, the average height of the oxygen atoms was found to be 13.13 Å. The substantial distance of the carboxyl group from the surface suggests that it contributes minimally to the adsorption process. Although the carbon atoms were positioned relatively closer to the surface, no strong overall binding was observed for the molecule.

In the C5 conformation, the average height of the oxygen atoms was calculated as 10.37 Å, while the carbon atoms were positioned at a height of 9.91 Å. The distant positioning of all atoms from the surface resulted in a less negative adsorption energy, indicating weaker interactions with the surface.

Overall, the results obtained demonstrate that the positioning of the carboxyl group close to the surface is a determining factor for the adsorption energy (Figure 8). Additionally, the parallel or tilted orientation of the phenyl group also contributes to the strength of the molecule-surface interactions, enhancing the stability of the system. Specifically, it has been shown that in the C2 conformation, the carboxyl group tightly binds to the surface, the overall structure of the molecule is parallel to the surface, and consequently, the lowest adsorption energy is achieved. In the visualization presented in Figure 7, the average and minimum heights of the oxygen (O) and carbon (C) atoms from the surface for each conformation are clearly compared. The graph clearly indicates that, particularly in the C2 conformation, both the oxygen and carbon atoms are positioned closer to the surface compared to the other conformations. This situation visually supports the reasoning that C2 is more stable. Notably, in the C4 and C5 conformations, the oxygen atoms are distinctly farther from the surface.

As a result, the adsorption energies on the Cu surface are more negative compared to those on the Al surface. For the conformations on the Cu surface, the adsorption energies range from −43.98 to −73.27 kcal/mol, with the most stable structure being the second conformation, which has an energy value of −73.27 kcal/mol. The other four conformations exhibit strong adsorption energies, ranging from −43.98 to −67.23 kcal/mol. Considering these results, it is evident that the adsorption of the PSCCA molecule on the Cu surface is stronger than on the Al surface. In particular, the higher negative adsorption energies on the Cu surface indicate that the interactions between the molecule and the surface are stronger, making the system thermodynamically more stable. This may be attributed to the Cu surface's electronic structure and atomic arrangement, which facilitate more effective bonding interactions with the molecule. The electronic structure of copper and its d-band electrons may enable stronger interactions with organic molecules [25]. Moreover, it is believed that the potential covalent and electrostatic interactions between the Cu surface and the carboxyl group and phenyl ring are more pronounced compared to those on the Al surface.

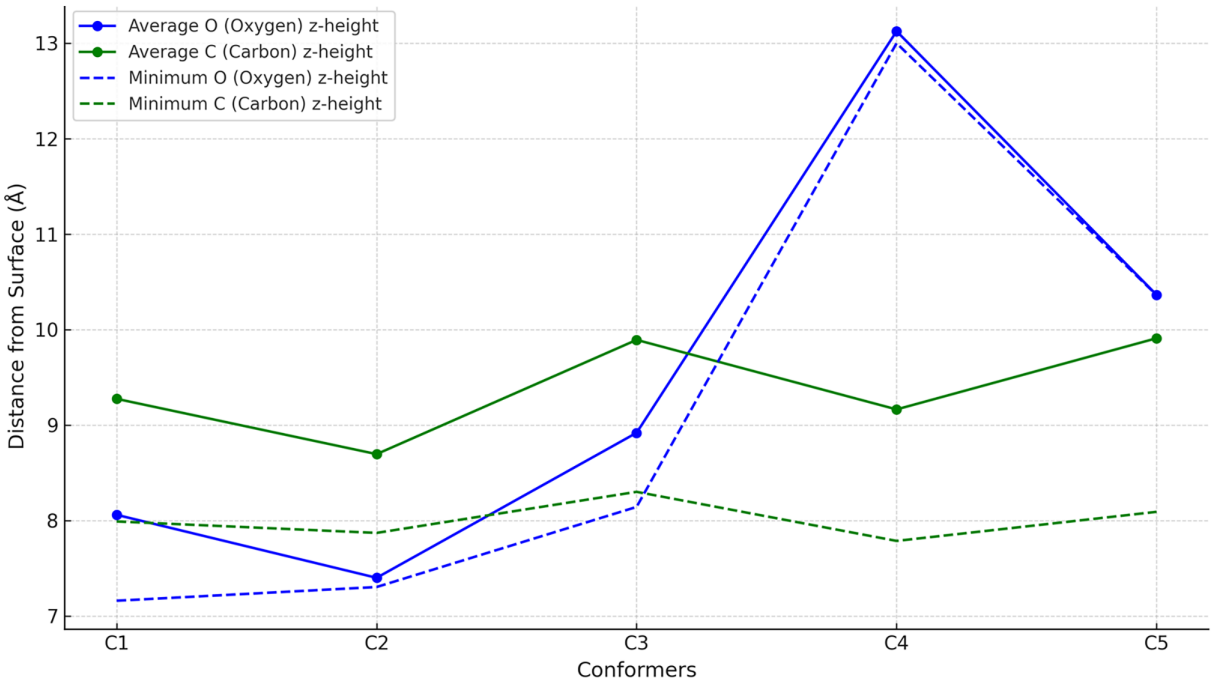

FIGURE 8 | Distance of O and C atoms relative to Al(111) surface.

3.5 | Atomic Distance and Adsorption Behavior of the PSCCA Molecule on the Cu(111) Surface

As a result of the optimizations, four different conformations (C1, C2, C3, and C5) were examined. The average and minimum heights of the oxygen (O) and carbon (C) atoms from the surface were calculated, and the molecule-surface interactions were evaluated. The findings are presented in Table 9.

Among all conformations, the most stable structure was determined to be the C2 conformation. The C2 conformation has the lowest oxygen atom height on the Cu(111) surface (average 6.73 Å, minimum 6.29 Å). This indicates that the carboxyl group is positioned very close to the surface and forms strong interactions. The average height of the carbon atoms is also quite low (7.59 Å), suggesting that the molecule adopts a parallel/tilted position relative to the surface. As a result of the molecule being positioned close to the surface in a balanced manner, it is expected to be the structure with the lowest adsorption energy. In the C1 conformation, the average distance of the oxygen atoms from the surface is found to be 7.12 Å, with the minimum oxygen height at 6.45 Å, which is slightly higher than in C2. The average height of carbon atoms is 7.68 Å. In the C3 conformation, the oxygen atoms are noticeably positioned farther from the surface (average 7.62 Å, minimum 7.02 Å). The carbon atoms are at a height of 8.39 Å, and the molecule is positioned more perpendicularly and farther from the surface. This results in less negative adsorption energy. In the C4 conformation, the average height of the carbon atoms is 8.30 Å, and the oxygen atoms are located farther from the surface, indicating that the molecule has weak interactions with the surface overall. In the C5 conformation, the average height of the oxygen atoms is 8.54 Å, and the carbon atoms are at 8.26 Å. The molecule is positioned farther from the surface, and the carboxyl group is unable to form effective bonding interactions. The most stable structure on the Cu surface is the C2 conformation. This structure stands out due to both the proximity of the oxygen atoms of the carboxyl group to the surface and the tilted/parallel positioning of the molecule relative to the surface. In the other conformations, the distance of the oxygen atoms from the surface increases, weakening the molecule–surface interactions. Particularly in the C5 and C3 structures, it can be observed that the potential for the carboxyl group to bind to the surface decreases, leading to a reduction in the overall stability of the molecule. The visualization results are provided in Figure 9. The graph clearly shows that, particularly in the C2 conformation, both the oxygen and carbon atoms are positioned closer to the surface compared to the other conformations. This visually supports the reasoning that C2 is more stable. In particular, the oxygen atoms in the C4 and C5 conformations are clearly positioned farther from the surface.

Table 10 below presents a comparative analysis of the adsorption properties of the PSCCA molecule on the Cu(111) and Al(111) surfaces.

As a result of the calculations performed on the Cu(111) and Al(111) surfaces, it has been observed that the distances of the oxygen atoms from the surface differ between the two surfaces. On the Cu surface, the oxygen atoms are generally positioned at lower heights compared to the Al surface. The lowest oxygen atom height on the Cu surface ranges from 6.29 to 7.72 Å, whereas on the Al surface, this range is between 7.16 and 10.36 Å. Specifically, in the C2 conformation, the distance of the oxygen atoms from the surface on the Cu surface has been calculated to be a minimum of 6.29 Å, indicating that this is the structure positioned closest to the surface. The distances of the carbon atoms from the surface are also lower on the Cu surface. The average carbon atom height on the Cu surface ranges from 7.59 to 8.39 Å, whereas on the Al surface, these values range from 8.70 to 9.91 Å. This indicates that the PSCCA molecule binds

TABLE 9 | Distances of O and C atoms and molecular *Z* values for Cu–ligand complexes.

Conformation	Average O atom height (Å)	Minimum O atom height (Å)	Average C atom height (Å)	Minimum C atom height (Å)	Minimum molecular Z (Å)	Maximum molecular Z (Å)
c1	7.12	6.45	7.68	6.72	6.26	10.11
c2	6.73	6.29	7.59	6.72	6.29	10.29
c3	7.62	7.02	8.39	7.06	5.97	11.42
c4	12.44	12.39	8.30	6.73	6.73	13.55
c5	8.54	7.72	8.26	7.11	6.08	10.57

Note: Z-axis: This is the axis perpendicular to the surface, indicating the vertical positioning of the molecule relative to the surface, that is, how far the molecule is located above or below the surface. Minimum Molecular *Z* (Å): This refers to the *z*-coordinate of the atom in the molecule that is closest to the surface (the atom at the lowest height). Maximum Molecular *Z* (Å): This refers to the *z*-coordinate of the atom in the molecule that is farthest from the surface (the atom at the highest position).

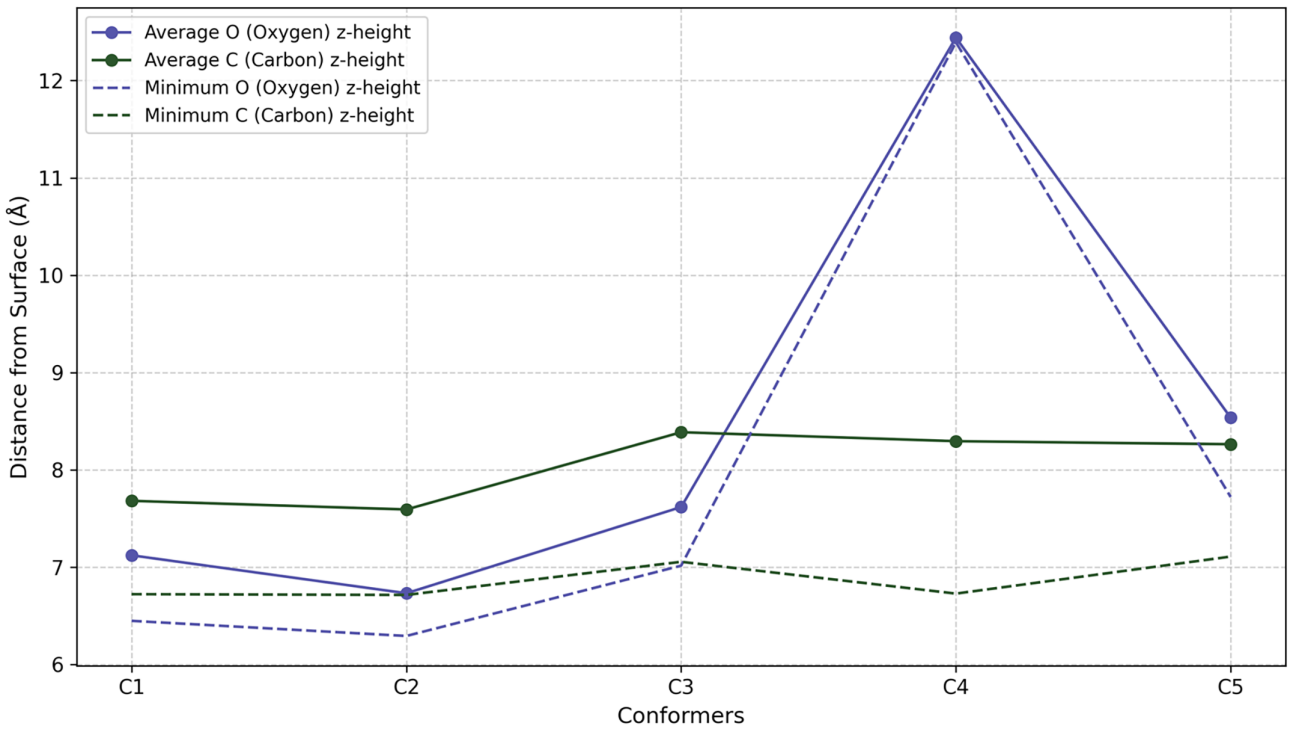

FIGURE 9 | Distance of O and C atoms relative to Cu(111) surface.

TABLE 10 | Distances of O and C atoms on Al and Cu surfaces for various conformers.

Conformation	Al surface average O atom distance (Å)	Al surface minimum O atom distance (Å)	Al surface average C atom distance (Å)	Al surface minimum C atom distance (Å)	Cu surface average O atom distance (Å)	Cu surface minimum O atom distance (Å)	Cu surface average C atom distance (Å)	Cu surface minimum C atom distance (Å)
c1	8.06	7.16	9.28	7.99	7.12	6.45	7.68	6.72
c2	7.40	7.30	8.70	7.87	6.73	6.29	7.59	6.72
c3	8.92	8.14	9.89	8.30	7.62	7.02	8.39	7.06
c4	13.13	13.00	9.16	7.79	12.44	12.39	8.30	6.73
c5	10.37	10.36	9.91	8.09	8.54	7.72	8.26	7.11

more strongly to the Cu surface compared to the Al surface, and the molecule is positioned closer to the surface. Based on the comparisons for both surfaces, it has been determined that the most stable conformation on both surfaces is C2. On the Cu surface, the approach of the oxygen atoms towards the surface in the C2 conformation (minimum 6.29 Å) is more pronounced compared to the Al surface, indicating a stronger interaction between the molecule and the surface. This positioning results in a more negative adsorption energy and leads to a more stable system.

TABLE 11 | Mulliken-based charge transfer analysis for ligand adsorption on Al(111) and Cu(111) surfaces.

Fragment	System (isolated) (e)	System (adsorbed) (e)	Charge transfer ΔQ (e)
Al(111) + ligand complex			
Ligand	−1.00E−06	0.211452	0.211453
Al(111) surface	3	2.788547	−0.211453
Cu(111) + ligand complex			
Ligand	−1E−06	0.581548	0.581549
Cu(111) surface	2.999999	2.418454	−0.581545

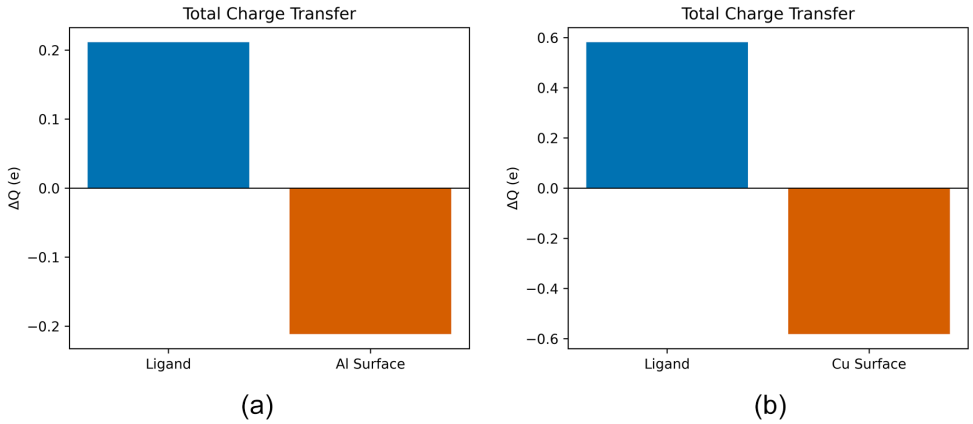

FIGURE 10 | Total charge transfer (ΔQ) for (a) Al(111) and (b) Cu(111) surfaces.

3.6 | Atomic-Scale Charge Transfer Analysis of Ligand–Metal Surface Interactions Using Mulliken Population

The Mulliken population analysis was performed based on the optimized C2 conformer of the ligand adsorbed on Al(111) and Cu(111) surfaces to investigate the electronic charge redistribution induced by adsorption (Table 11). The atom-resolved charge transfer results are presented in Figure 10, where the top 10 atoms with the largest Mulliken charge changes (ΔQ) are displayed for each fragment.

Upon adsorption of the ligand onto the Al(111) surface, a net charge transfer of +0.211 e to the ligand fragment was observed, while the Al(111) surface exhibited a corresponding depletion of −0.211 e. This result indicates a moderate electron donation from the Al surface to the ligand during adsorption. The charge redistribution suggests the formation of weak to moderate donor–acceptor interactions between the ligand and the Al(111) surface, most likely dominated by surface states interacting with the ligand's frontier molecular orbitals.

In contrast, a significantly larger charge transfer was calculated for the Cu(111) surface. The ligand gains approximately +0.581 e upon adsorption, while the Cu(111) surface loses an equivalent amount of charge (−0.581 e). This substantial increase in charge transfer for the Cu(111) surface can be attributed to the enhanced electronic coupling between the Cu d-band and the ligand orbitals, facilitating stronger electron donation mechanisms. The higher density of states near the Fermi level in Cu compared to Al likely contributes to this increased electronic interaction. The comparison of Al(111) and Cu(111) surfaces clearly demonstrates that the nature of the metal surface plays a critical role in determining the extent of electronic charge redistribution during ligand adsorption. The Cu(111) surface exhibits nearly 2.75 times higher charge transfer compared to Al(111), suggesting stronger chemisorption characteristics for Cu. This finding may have important implications for catalytic, sensing, and electronic applications where surface-ligand interactions are crucial for functionality. These results are consistent with the general trends described by the d-band model of surface reactivity, which predicts that metal surfaces with partially filled d-states (such as Cu) facilitate stronger adsorption-induced charge transfer due to enhanced orbital hybridization with adsorbed species [26]. Mulliken population analysis was performed to investigate the electronic charge redistribution induced by ligand adsorption on Al(111) and Cu(111) surfaces. The atom-resolved charge transfer results are presented in Figures 11 and 12, where the top 10 atoms with the largest Mulliken charge changes (ΔQ) are displayed for each fragment.

Upon adsorption onto the Al(111) surface, the ligand exhibits moderate charge redistribution. The maximum charge accumulation was observed on electronegative atoms such as C3 and O2, which gained approximately +0.033 e. Conversely, several hydrogen atoms exhibited charge depletion up to −0.02 e, indicating limited electronic polarization within the ligand upon interaction with the Al surface. For the Al surface atoms, the maximum charge variation reached approximately ±0.04 e, with Al72 showing the largest depletion (−0.055 e) and Al117 displaying charge accumulation (+0.038 e). This localized redistribution suggests weak electronic coupling between the ligand and the Al surface,

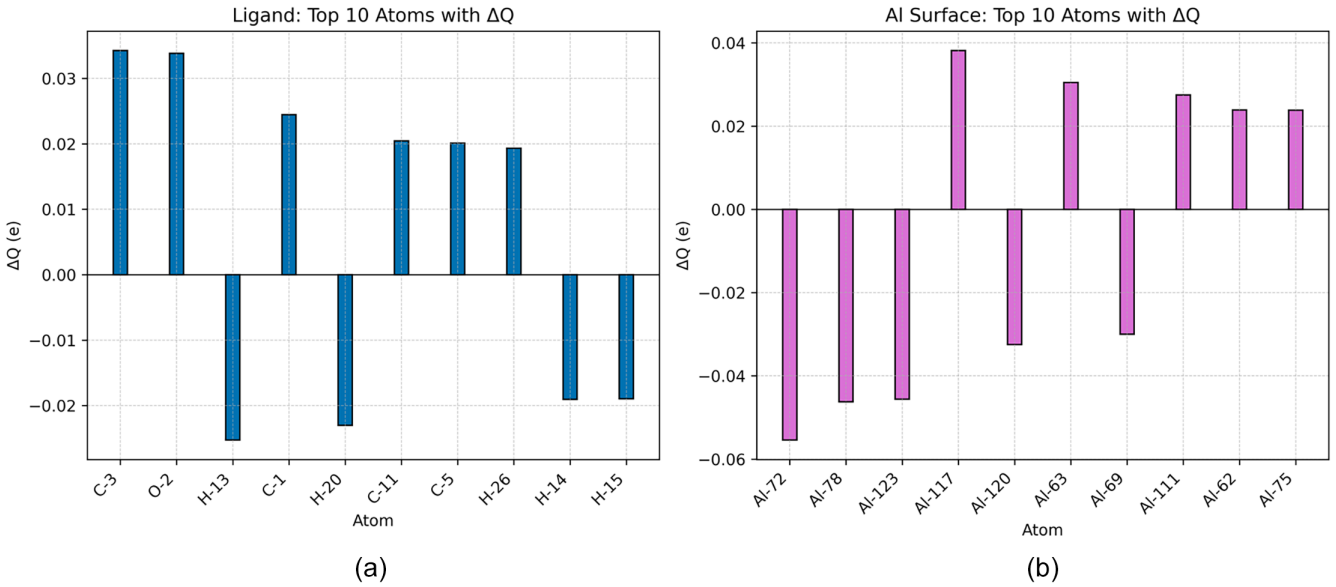

FIGURE 11 | Atom-resolved Mulliken charge transfer upon ligand adsorption on Al(111) surface. (a) Ligand atoms; (b) Al surface atoms. The top 10 atoms with the largest ΔQ values are displayed for each fragment.

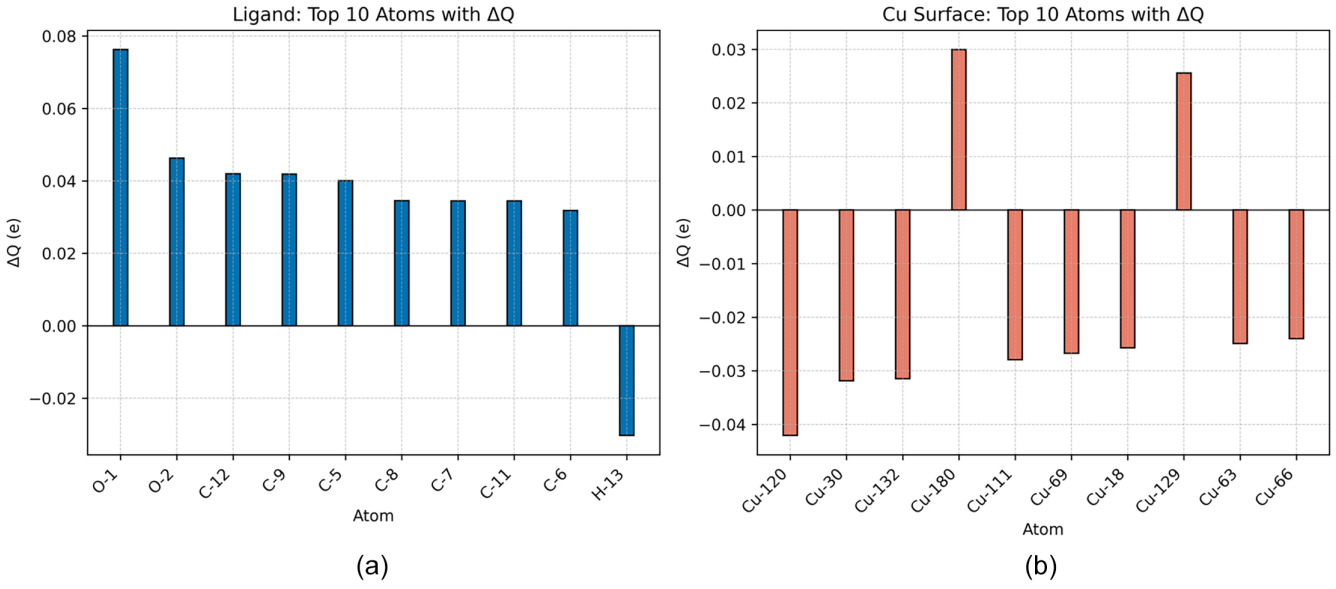

FIGURE 12 | Atom-resolved Mulliken charge transfer upon ligand adsorption on Cu(111) surface. (a) Ligand atoms; (b) Cu surface atoms. The top 10 atoms with the largest ΔQ values are displayed for each fragment.

consistent with physisorption or weak chemisorption behavior. In contrast, adsorption on the Cu(111) surface resulted in substantially stronger charge redistribution. The ligand atoms experienced charge accumulations up to +0.08 e, primarily localized on the oxygen atoms (O1, O2), while hydrogen atoms exhibited charge depletion in the range of −0.03 e. For Cu surface atoms, the maximum charge variations were slightly smaller, around ±0.03 e, with Cu132 losing −0.025 e and Cu180 gaining +0.03 e. Compared to Al, the charge redistribution on the Cu surface was more evenly distributed across several surface atoms. The overall results clearly demonstrate that ligand adsorption on Cu(111) induces substantially greater charge transfer than on Al(111). This difference originates from the distinct electronic structures of the two metals. The partially filled d-band of Cu allows for stronger orbital hybridization and enhanced electronic coupling with the ligand's frontier orbitals, while the s–p band of Al limits such interactions. As a result, Cu(111) promotes more efficient electron donation to the ligand, resulting in stronger adsorption and greater charge redistribution.

In particular, the observed charge transfer difference at the O1 atom between Al(111) and Cu(111) systems can be directly attributed to this electronic structure effect. On Al(111), the relatively low d-band density of states does not provide sufficient orbital alignment and hybridization with the lone pair electrons of the O1 atom, resulting in a minor charge transfer of approximately +0.010 e. In contrast, the high d-band density of Cu(111) enables more effective orbital overlap with the O1 lone

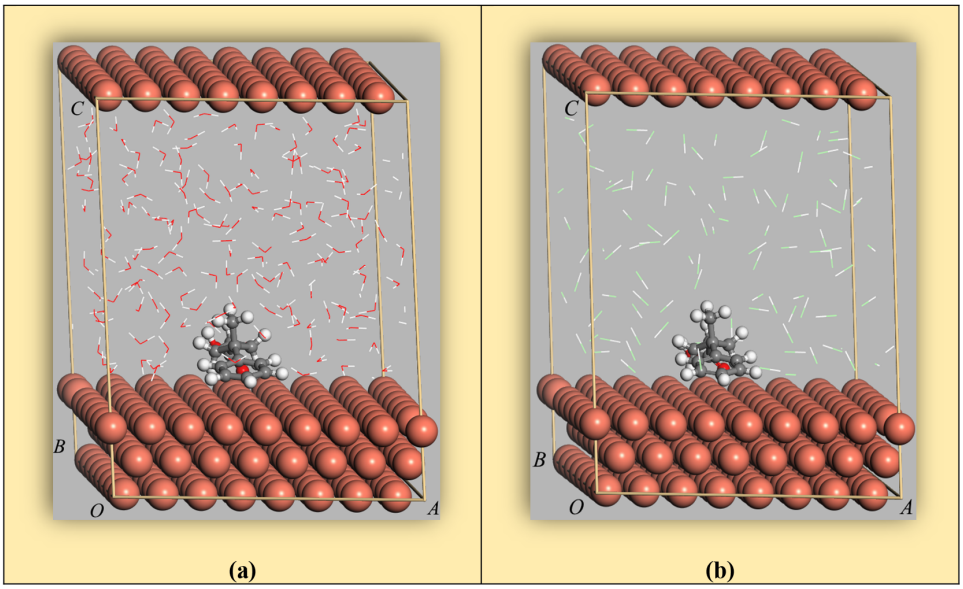

FIGURE 13 | Visualization of the system showing the adsorption of the PSCCA molecule on the Al(111) surface and the distribution of surrounding (a) H_2O and (b) HCl molecules.

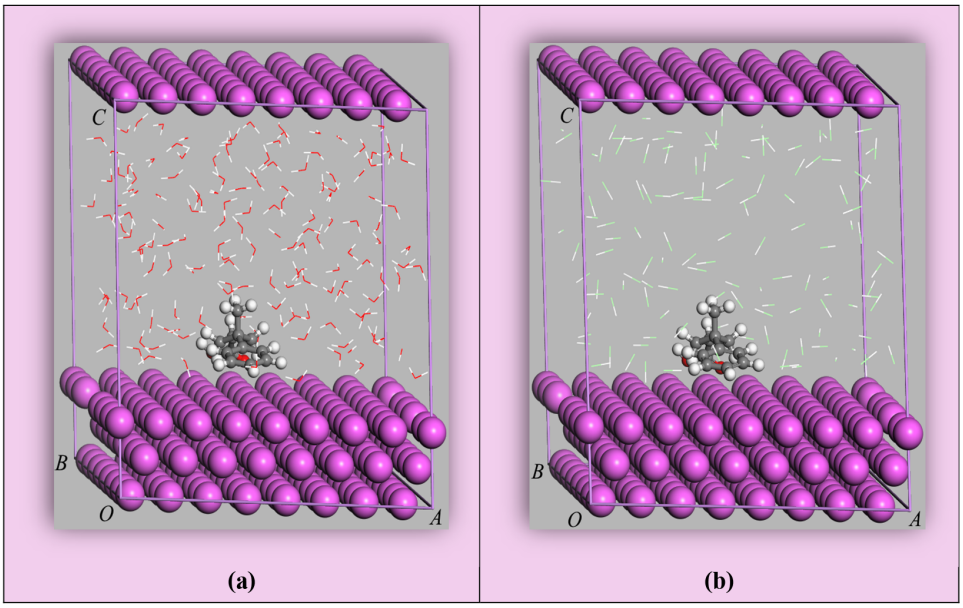

FIGURE 14 | Visualization of the system showing the adsorption of the PSCCA molecule on the Cu(111) surface and the distribution of surrounding (a) H_2O and (b) HCl molecules.

pair, leading to a significant charge transfer exceeding +0.08 e. These findings are consistent with the predictions of the d-band model, which correlates the metal's d-band center position with its adsorption strength and charge transfer capacity [27].

3.7 | Adsorption Energies of the Compound on Al and Cu Surfaces With H_2O and HCl

The adsorption of the PSCCA molecule on Al and Cu surfaces in the presence of water (H_2O) and hydrochloric acid (HCl) molecules has been investigated (Figures 13 and 14). In both systems, C2 conformations were used. On the Al surface, in the presence of a water molecule, the adsorption energy was calculated to be −68.63 kcal/mol (Table 12). Water molecules may facilitate adsorption by forming hydrogen bonds with the carboxyl group or by altering the hydration layer on the aluminum surface [28].

This value indicates that the bonding between the molecule and the Al surface becomes more stable due to the presence of the water molecule. The adsorption energy in the presence of the HCl molecule was found to be −64.10 kcal/mol. Although this result is slightly lower than that with water, it still indicates strong adsorption on the Al surface. The presence of HCl may affect the adsorption by causing protonation of the carboxyl

TABLE 12 | Adsorption energies of PSCCA on Al(111) surface in the presence of H_2O and HCl.

System	$E_{Al+lig+H2O}$	E_{Al+H2O}	E_{lig}	ΔE (kcal/mol)
Al(111)/PSCCA/H_2O	−3090.68971	−2981.954009	−108.6263306	−68.6305
Al(111)/PSCCA/HCl	−2532.59589	−2423.865639	−108.6280968	−64.1023

TABLE 13 | Adsorption Energies of PSCCA on Cu(111) Surface in the Presence of H_2O and HCl.

System	$E_{Cu+lig+H2O}$	E_{Cu+H2O}	E_{lig}	ΔE (kcal/mol)
Cu(111)/PSCCA/H_2O	−11934.59483	−11825.79735	−108.6171133	−113.185
Cu(111)/PSCCA/HCl	−10908.11897	−10799.35434	−108.6262093	−86.8581

group or by promoting interactions between chloride ions and the surface [29].

When examining the Cu surface, the adsorption energy calculated in the presence of a water molecule reaches a significantly negative value of −113.18 kcal/mol.

This result indicates that the interaction between the molecule and the Cu surface is significantly enhanced through the presence of the water molecule, leading to a highly stable system. In the presence of the HCl molecule, the adsorption energy on the Cu surface was found to be −86.86 kcal/mol (Table 13). This value is lower than the complex formed with H_2O on the Cu surface, but more negative compared to the complexes on the Al surface.

The adsorption behavior of the PSCCA molecule on aluminum (Al) and copper (Cu) surfaces has been investigated under the presence and absence of water (H_2O) and hydrochloric acid (HCl) molecules. As a result, on the Al surface, adsorption energies without solvent molecules range from −17.89 to −39.12 kcal/mol. This indicates that the interactions between the molecule and the Al surface are of moderate strength. However, in the presence of H_2O, the adsorption energy decreases to −68.63 kcal/mol, and in the presence of HCl, it decreases to −64.10 kcal/mol. These results show that water and HCl molecules significantly enhance adsorption on the Al surface, making the system more stable. On the Cu surface, adsorption energies without solvents range from −43.97 to −73.27 kcal/mol, indicating strong interactions between the molecule and the Cu surface. In the presence of H_2O, the adsorption energy decreases to −113.18 kcal/mol, and in the presence of HCl, it decreases to −86.86 kcal/mol. These findings indicate that the presence of the water molecule significantly strengthens the interactions between the Cu surface and the molecule, making the system more stable. Overall, the presence of water and HCl molecules on both surfaces shifts the adsorption energies to more negative values, thus stabilizing the system. In particular, the water molecule is more effective in increasing the adsorption stability on both surfaces. Furthermore, the Cu surface forms more stable adsorption complexes with the molecule by establishing stronger interactions compared to the Al surface. In the existing literature, adsorption energies of similar organic molecules on metal surfaces are generally reported to range from −10 to −50 kcal/mol. For instance, a study on the adsorption of methyl orange using potassium permanganate-coated zeolite and iron oxide-coated zeolite reported adsorption capacities of 14.3 and 12.6 mg/g, respectively [29]. In this context, the adsorption energies obtained in our study are consistent with those reported in the literature, with some cases showing higher adsorption energies. In particular, the adsorption energy of −113.18 kcal/mol on the Cu surface in the presence of water emphasizes the significant role of water molecules in the adsorption process.

In the current literature, adsorption energies of similar organic molecules on metal surfaces are generally reported to range from −10 to −50 kcal/mol [30]. For example, the adsorption energies of organophosphorus compounds on transition metal-doped activated carbons have been reported to be above 43 kcal/mol [31]. In another study, the binding energies of NO and CO on Ag-doped metal–organic frameworks (MOFs) were reported to be around −21 to −26 kcal/mol [32]. It is also noted that typical adsorption energies for physical adsorption usually do not exceed 20–25 kJ/mol (approximately 4.8–6 kcal/mol) [33]. When the obtained adsorption energies are compared to similar studies in the literature, it is observed that the type of metal surface, the structure of the organic molecule, and the effect of the solvent significantly influence the adsorption energies.

4 | Conclusion

In this study, the structural identity of PSCCA was successfully confirmed through NMR, IR, and X-ray crystallography techniques. The optimized molecular geometry obtained via DFT calculations provided a reliable model for further adsorption studies. Comprehensive first-principles calculations were performed to investigate the adsorption behavior of PSCCA on Al(111) and Cu(111) surfaces using the CP2K framework. The adsorption energies of PSCCA on both metal surfaces indicated favorable interactions, with notably stronger adsorption on the Cu surface. Specifically, the most stable adsorption configuration on Cu(111) exhibited an adsorption energy of −73.27 kcal/mol, compared to −39.12 kcal/mol on Al(111). These results highlight the critical influence of the metal type on the adsorption strength and suggest a higher affinity of PSCCA for Cu surfaces. Analysis of molecular orientations revealed that the proximity and alignment of the carboxyl group and phenyl ring significantly impacted the adsorption energy and stability. Additionally, the presence of water (H_2O) and hydrochloric acid (HCl) molecules was found to enhance the adsorption stability on both surfaces. The adsorption energy reached −113.18 kcal/mol for Cu(111) in the presence of water, demonstrating a remarkable increase in interaction strength. This emphasizes the role of solvent molecules

in modulating surface-molecule interactions, which could be exploited in practical applications such as corrosion inhibition, catalysis, and sensor development. Overall, the combined experimental and theoretical findings of this study not only deepen the understanding of PSCCA's surface adsorption behavior but also provide valuable insights for the rational design of functional metal–organic interfaces in materials science and surface chemistry. In addition, atomic-scale charge transfer analysis based on Mulliken population calculations provided critical insight into the nature of ligand–metal interactions. Adsorption on the Al(111) surface resulted in limited charge transfer (+0.211 e), reflecting weak donor-acceptor interactions primarily governed by the low d-band density of Al. In sharp contrast, the Cu(111) surface exhibited a substantially larger charge transfer (+0.581 e), driven by strong orbital hybridization between the ligand's frontier orbitals and the partially filled Cu d-band. This nearly 2.75-fold enhancement in electron transfer on Cu(111) directly correlates with its superior adsorption strength, as confirmed by the computed adsorption energies. These findings not only highlight the dominant role of metal electronic structure in controlling adsorption phenomena but also offer valuable guidance for tailoring metal–organic interfaces in applications such as catalysis, corrosion inhibition, and surface-based sensing technologies.

Data Availability Statement

All data generated or analyzed during this study are included in this published article.

References

1. F. Gnad and O. Reiser, "Synthesis and Applications of β-Aminocarboxylic Acids Containing a Cyclopropane Ring," *Chemical Reviews* 103 (2003): 1603–1624.

2. M. Laktsevich-Iskryk, A. Hurski, M. Ošeka, and D. Kananovich, "Recent Advances in Asymmetric Synthesis via Cyclopropanol Intermediates," *Organic & Biomolecular Chemistry* 23 (2025): 992–1015.

3. S.-Y. Li, S. Yuan, X. M. Zhao, Q. Wang, J. Zhu, and S.-C. Zheng, "Highly Diastereoselective and Enantioselective Cyclopropanation of Alkenes Catalyzed by a Chiral Iridium(III) Porphyrin Complex," *Chem Catalysis* 5 (2025): 101262.

4. W.-W. Chen and M.-H. Xu, "Recent Advances in Rhodium-Catalyzed Asymmetric Synthesis of Heterocycles," *Organic & Biomolecular Chemistry* 15 (2017): 1029–1050.

5. L. A. Wessjohann, W. Brandt, and T. Thiemann, "Biosynthesis and Metabolism of Cyclopropane Rings in Natural Compounds," *Chemical Reviews* 103 (2003): 1625–1648.

6. S. Bruker and S. Saint, *SAINT Software User's Guide* (Bruker AXS Inc., 2002).

7. G. M. Sheldrick, "SHELXT–Integrated Space-Group and Crystal-Structure Determination," *Acta Crystallogr* 71 (2015): 3–8.

8. G. M. Sheldrick, "Crystal Structure Refinement with SHELXL," *Acta Crystallographica Section C: Structural Chemistry* 71 (2015): 3–8.

9. O. V. Dolomanov, L. J. Bourhis, R. J. Gildea, J. A. Howard, and H. Puschmann, "OLEX2: A Complete Structure Solution, Refinement and Analysis Program," *Journal of Applied Crystallography* 42 (2009): 339–341.

10. M. A. Akhmedov, I. K. Sardarov, I. M. Akhmedov, R. R. Kostikov, A. V. Kisin, and N. M. Babaev, "Formation of Substituted-Cyclobutanes In the Reaction of 2-(2-Methyl-2-propenyl)-3-Chloromethyloxirane with Aromatic-Hydrocarbons," *Zhurnal Organicheskoi Khimii* 27 (1991): 1434–1440.

11. T. D. Kühne, M. Iannuzzi, M. Del Ben, et al., "CP2K: An Electronic Structure and Molecular Dynamics Software Package," *Journal of Chemical Physics* 152 (2020): 194103.

12. S. Grimme, J. Antony, S. Ehrlich, and H. Krieg, "A Consistent and Accurate Ab Initio Parametrization of Density Functional Dispersion Correction (DFT-D3)," *Journal of Chemical Physics* 132 (2010): 154104.

13. J. P. Perdew, K. Burke, and M. Ernzerhof, "Generalized Gradient Approximation Made Simple," *Physical Review Letters* 77 (1996): 3865–3868.

14. J. VandeVondele and J. Hutter, "Gaussian Basis Sets for Accurate Calculations on Molecular Systems in Gas and Condensed Phases," *Journal of Chemical Physics* 127 (2007): 114105.

15. F. H. Allen, O. Kennard, D. G. Watson, L. Brammer, A. G. Orpen, and R. Taylor, "Tables of Bond Lengths Determined by X-ray and Neutron Diffraction. Part 1. Bond Lengths in Organic Compounds," *Journal of the Chemical Society, Perkin Transactions* 2 (1987): S1–S19.

16. H. B. Buergi and J. D. Dunitz, "From Crystal Statics to Chemical Dynamics," *Accounts of Chemical Research* 16 (1983): 153–161.

17. L. Rigamonti and A. Forni, "Effect of Crystal Packing and Coordinated Solvent Molecules on Metal-Ligand Bond Distances in Linear Trinuclear Nickel Compounds With Bridging Acetato and Schiff Base Ligands," *Inorganica Chimica Acta* 473 (2018): 216–222.

18. G. Aullón, D. Bellamy, A. G. Orpen, L. Brammer, and E. A. Bruton, "Metal-Bound Chlorine Often Accepts Hydrogen Bonds," *Chemical Communications* 6 (1998): 653–654.

19. M. Dewar and H. Schmeising, "A Re-Evaluation of Conjugation and Hyperconjugation: The Effects of Changes in Hybridisation on Carbon Bonds," *Tetrahedron* 5 (1959): 166–178.

20. F. A. Cotton, G. Wilkinson, C. A. Murillo, and M. Bochmann, *Advanced Inorganic Chemistry* (John Wiley & Sons, 1999).

21. L. Bartell, "On The Effects of Intramolecular Van Der Waals Forces," *Journal of Chemical Physics* 32 (1960): 827–831.

22. L. O. Mark, C. Zhu, J. W. Medlin, and H. Heinz, "Understanding the Surface Reactivity of Ligand-Protected Metal Nanoparticles for Biomass Upgrading," *ACS Catalysis* 10 (2020): 5462–5474.

23. M. Poberžnik, F. Chiter, I. Milošev, P. Marcus, D. Costa, and A. Kokalj, "DFT Study of n-Alkyl Carboxylic Acids on Oxidized Aluminum Surfaces: From Standalone Molecules to Self-Assembled-Monolayers," *Applied Surface Science* 525 (2020): 146156.

24. W. Reckien, M. Eggers, and T. Bredow, "Theoretical Study of the Adsorption of Benzene on Coinage Metals," *Beilstein Journal of Organic Chemistry* 10 (2014): 1775–1784.

25. W. Gao, Y. Chen, B. Li, S.-P. Liu, X. Liu, and Q. Jiang, "Determining the Adsorption Energies of Small Molecules With the Intrinsic Properties of Adsorbates and Substrates," *Nature Communications* 11 (2020): 1196.

26. B. J. K. N. Hammer and J. K. Nørskov, "Electronic Factors Determining the Reactivity of Metal Surfaces," *Surface Science* 343, no. 3 (1995): 211–220.

27. J. K. Nørskov, J. Rossmeisl, A. Logadottir, et al., "Origin of the Overpotential for Oxygen Reduction at a Fuel-Cell Cathode," *Journal of Physical Chemistry B* 108, no. 46 (2004): 17886–17892.

28. R. M. Giappa, A. G. Papadopoulos, E. Klontzas, E. Tylianakis, and G. E. Froudakis, "Linker Functionalization Strategy for Water Adsorption in Metal–Organic Frameworks," *Molecules* 27 (2022): 2614.

29. A.-R. El-Sayed, M. M. El-Hendawy, M. S. El-Mahdy, F. S. Hassan, and A. E. Mohamed, "The Inhibitive Action of 2-Mercaptobenzothiazole on the Porosity of Corrosion Film Formed on Aluminum and

Aluminum–Titanium Alloys in Hydrochloric Acid Solution," *Scientific Reports* 13 (2023): 4812.

30. D. Gümüş and F. Gümüş, "Potasyum Permanganat Kaplı Zeolit ve Demir Oksit Kaplı Zeolitle Metil Oranjın Adsorpsiyon Çalışmaları," *Kahramanmaraş Sütçü İmam Üniversitesi Mühendislik Bilimleri Dergisi* 21 (2018): 43–54.

31. J. Claudot, E. Soubeyrand-Lenoir, and G. Maurin, "Competitive Adsorption of Water and Chemical Warfare Agents on Transition Metal Embedded Graphene," *Applied Surface Science* 551 (2021): 149433.

32. S. Naderlou, M. Vahedpour, and D. M. Franz, "Multi-Scale Computational Investigation of Ag-Doped Two-Dimensional Zn-Based MOFs for Storage and Release of Small NO and CO Bioactive Molecules," *Physical Chemistry Chemical Physics* 25 (2023): 2830–2845.

33. R. J. Maurer, V. G. Ruiz, J. Camarillo-Cisneros, et al., "Adsorption Structures and Energetics of Molecules on Metal Surfaces: Bridging Experiment and Theory," *Progress in Surface Science* 91 (2016): 72–100.